Design and Analysis Framework for Linear Permanent-Magnet Machines

David L. Trumper, *Member, IEEE,* Won-jong Kim, *Student Member, IEEE,* and Mark E. Williams

Abstract—**This paper presents a design and analysis framework for the general class of permanent-magnet electric machines. In our analysis, surface-mounted linear motors consisting of permanent magnets and iron-less current-carrying coils are treated in a uniform way via the magnetic vector potential. This analysis is developed to design novel linear magnetic levitators for driving precision motion control stages such as those used in wafer steppers. For one such motor structure we give analytical formulae for its magnetic field, force, flux linkage, inductance of the winding, and back electromotive force. We provide experimental results with a six-degree-of-freedom magnetic levitator. These results are in good agreement with analytical estimations. The levitator uses a permanent-magnet Halbach array in order to improve its power efficiency. By analogy, there also exists an electromagnetic dual of the Halbach array. One such dual utilizes a triangular winding pattern in order to achieve a primarily single-sided magnetic field.**

I. Introduction

THE control of motion in the near-vicinity of a plane is an important task in many precision machines, e.g., wafer steppers, surface profilometers, and scanned probe microscopes. In the case of wafer stepper stages, which are the primary focus of our work, the motion control stage must provide travel over relatively large displacements (hundreds of millimeters) in two planar degrees of freedom, small displacements (hundreds of micrometers) in the direction normal to the plane, as well as small rotational displacements (milliradians) about three orthogonal axes.

The work described in this paper is motivated by the desire to develop analytical tools to facilitate the design of a stage which can provide the above ranges of motion with only a single magnetically-levitated moving part. Our approach promises significant advantages for the wafer stepper application. Among these advantages are the following: 1) A single moving part can be designed to have high natural frequencies and thus can be moved rapidly vis-a-vis multi-element stages which have more complex dynamics. This allows increased machine throughput. 2) The accuracy of a magnetically levitated stage is not limited by its bearing surfaces, and thus our design can scale with the decreasing feature sizes of next-generation integrated circuits. 3) A fully levitated stage requires no precision bearing surfaces, which thereby reduces fabrication cost. 4) A levitated stage requires no lubricants and does not generate wear particles, and is thus highly suited for clean-room or vacuum environments. 5) By eliminating complex mechanical elements the stage fabrication costs are reduced and the stage reliability is increased.

The key elements of any magnetically levitated stage are the actuators which apply controlled forces in order to stabilize the position of the stage. Since our stage requires significant planar travel, we have focused our design effort on the development of linear motors which are compatible with the motion requirements stated above. A promising motor structure utilizes permanent magnets on the moving stage which are driven by stator coils in the fixed machine base. This motor structure is the focus of the current paper. In order to choose the best motor topology, we have developed a set of analytical tools which allow the optimization of the linear motor design in terms of criteria such as packaging, force density, power efficiency, and winding pattern. These tools are presented in subsequent sections of this paper.

Many other researchers have studied the problem of the control of planar motion. An early example is the Sawyer motor given in [1]. This motor is a variable reluctance type and is used without any positioning feedback, i.e., as a stepper. The reported step resolution is on the order of 250 μm (0.01 in). Since the primary application is x-y plotters, 0.01-in resolution is sufficient. In the semiconductor industry, higher position resolution is required. To this end [2] and [3] present methods to improve the original version of the Sawyer motor for precision motion control with a particular emphasis on solutions used for wafer stepper stages. Keeping pace with advances of permanent-magnet material in the last decade, surface motor structures using permanent magnets are presented in [4]–[6]. Other planar movement systems are given in [7] and [8].

The permanent-magnet array we use in our motor is first presented by Halbach [9]. Such an array is also studied in [10], where it is represented by a two-dimensional multipole field expansion via complex variable theory. Abele and others represent the magnet array in spherical harmonics and calculated the coefficients [11].

In order to analyze permanent-magnet electric machines effectively, we have adopted an approach which can treat both magnetized material and winding current in a uniform fashion. Further, the results we derive herein can be used to analyze other types of machines. For instance, the motors we have developed are iron-free in order to remain compatible

Paper IPCSD 95–64, approved by the Electric Machines Committee of the IEEE Industry Applications Society for presentation at the 1994 IEEE Industry Applications Society Annual Meeting, Denver, CO, October 2–7. This work was supported by a contract from Sandia National Laboratories, and by a Korean Government Overseas Scholarship. Manuscript released for publication September 15, 1995.

The authors are with the Laboratory for Manufacturing and Productivity, Massachusetts Institute of Technology, Cambridge, MA 02139 USA

Publisher Item Identifier S 0093-9994(96)01581-2.

with magnetic suspension bearings. However, the transfer relations we present can be applied in the context of an iron-backed motor simply by changing boundary conditions. The development of these transfer relations is described in detail so that other researchers can adapt our analyses to their particular design objectives.

II. Magnetic Field Theory

For the theoretical aspects of this paper, we adopt Melcher's general methodology to describe electromagnetic phenomena with transfer relations [12]. Under magnetoquasistatic (MQS) assumptions [13] the time variation of electric field related quantities is insignificant. In this case, Maxwell's equations for magnetic field intensity $\mathbf{H}$, magnetic flux density $\mathbf{B}$, and electric field intensity $\mathbf{E}$ simplify to

$$\nabla \times \mathbf{H} = \mathbf{J}_f \tag{1}$$

$$\nabla \cdot \mathbf{B} = 0 \tag{2}$$

$$\nabla \times \mathbf{E} = -\frac{\partial \mathbf{B}}{\partial t} \tag{3}$$

where $\mathbf{J}_f$ is free volume current density due to the movement of free charges. The quantities $\mathbf{B}$ and $\mathbf{H}$ are related through magnetization $\mathbf{M}$ as

$$\mathbf{B} = \mu_0(\mathbf{H} + \mathbf{M}) \tag{4}$$

where $\mu_0 = 4\pi \times 10^{-7}$ H/m is the permeability of free space. We assume the permeability to be μ_0 everywhere since our design is iron-free. This assumption is reasonable even for permanent-magnet material like NdFeB since its relative permeability is near unity.

The boundary conditions which derive from (1) and (2) can be written as $\mathbf{n} \times [\mathbf{B}^a - \mathbf{B}^b] = \mu_0 \mathbf{K}_f + \mathbf{n} \times [\mu_0 \mathbf{M}^a - \mu_0 \mathbf{M}^b]$ and $\mathbf{n} \cdot [\mathbf{B}^a - \mathbf{B}^b] = 0$. Here, variables denoted a and b represent the associated quantities evaluated on opposite sides of a boundary. The vector $\mathbf{n}$ is normal to the boundary and points into the side labeled a. The variable $\mathbf{K}_f$ is a source surface current directed along the boundary. We further define $\mathbf{K}_e = \mathbf{n} \times [\mathbf{M}^a - \mathbf{M}^b]$; this can be thought of as an equivalent surface current which represents step discontinuities in the magnetization tangential to the boundary.

The magnetic flux density $\mathbf{B}$ can be represented with the magnetic vector potential $\mathbf{A}$ as $\mathbf{B} \equiv \nabla \times \mathbf{A}$. Since the divergence of the curl of a vector is identically zero, this representation automatically satisfies (2). Applying the curl operator to both sides yields

$$\nabla \times \mathbf{B} = \nabla \times \nabla \times \mathbf{A} = \nabla(\nabla \cdot \mathbf{A}) - \nabla^2 \mathbf{A}. \tag{5}$$

If we set the Coulomb gauge, $\nabla \cdot \mathbf{A} = 0$, this leads to

$$\nabla \times \mathbf{B} = -\nabla^2 \mathbf{A}. \tag{6}$$

However, via (1) and (4) we also have $\nabla \times \mathbf{B} = \mu_0(\mathbf{J}_f + \nabla \times \mathbf{M})$. Combining the last two results yields the vector Poisson equation

$$\nabla^2 \mathbf{A} = -\mu_0(\mathbf{J}_f + \nabla \times \mathbf{M}). \tag{7}$$

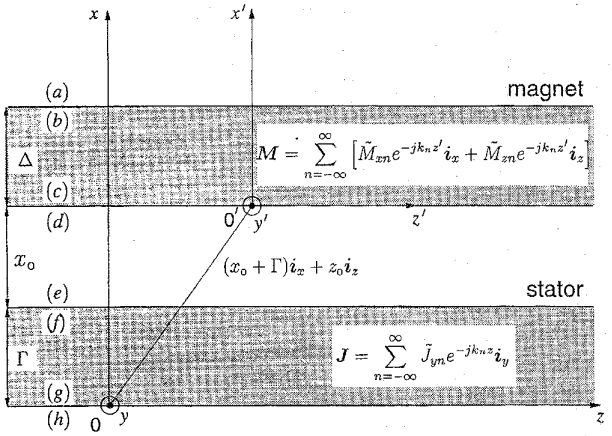

Fig. 1. Linear motor model.

In the above equation, $-\mu_0 \mathbf{J}_f$ represents the stator current. We can think of the term $-\mu_0 \nabla \times \mathbf{M}$ as an equivalent current which represents the magnet.

In two-dimensional cases where the fields lie in the xz-plane with no dependency on y, the vector potential is purely y-directed. In this case the vector Poisson equation simplifies to the scalar relationship

$$\frac{\partial^2}{\partial y^2} A_y = -\mu_0 \left(J_y + \frac{\partial}{\partial z} M_x - \frac{\partial}{\partial x} M_z \right). \tag{8}$$

This scalar equation is used in the analysis which follows.

III. Linear Machine Analysis

The geometry used to model the motor fields is shown in Fig. 1. Here the lower shaded region of thickness Γ represents the stator winding with y-directed current density $\mathbf{J}$, which is expressed as an infinite Fourier series. The upper shaded region of thickness Δ represents the magnet array, carrying a primed coordinate frame which is displaced from the base coordinate frame by a vector $(x_0 + \Gamma)\mathbf{i}_x + z_0 \mathbf{i}_z$. Thus x_0 is the motor air gap, and z_0 is the lateral displacement of the magnet array relative to the stator. The magnet array is represented by an infinite Fourier series in horizontal(z-directed) and vertical (x-directed) magnetization components through terms $\tilde{M}_{zn}$ and $\tilde{M}_{xn}$, respectively. A similar Fourier representation is also applied to $\mathbf{J}$, $\mathbf{B}$, $\mathbf{H}$, and $\mathbf{A}$. The pitch of the motor is l, and the spatial wavenumber of the nth harmonic is $k_n = 2\pi n/l$. We further define $\gamma_n = |k_n|$. The motor is assumed to be of depth w in the y-direction. End effects in this direction are neglected. Letters (a)–(h) represent the surfaces at the indicated boundaries.

A. Field Solutions

In earlier work [14], the field and force characteristics of a linear motor were analyzed via the magnetic scalar potential. Since the scalar potential is not unique in current-carrying volumes, the analysis therein uses a Green's function approach to calculate the field due to the stator. In contrast, in the present work we use the magnetic vector potential since it is

valid throughout both the permanent magnet and the current-carrying regions of the linear motor model. Use of the vector potential also simplifies the calculation of flux linkage in order to calculate coil inductance.

Extending results developed in [12], we show in Appendix A that the transfer relations which describe the model of Fig. 1 are

$$\tilde{B}^a_{zn} = -\gamma_n \tilde{A}^a_{yn} \tag{9}$$

$$\begin{bmatrix} \tilde{B}^b_{zn} \\ \tilde{B}^c_{zn} \end{bmatrix} = k_n \begin{bmatrix} \coth k_n\Delta & \frac{-1}{\sinh k_n\Delta} \\ \frac{1}{\sinh k_n\Delta} & -\coth k_n\Delta \end{bmatrix} \begin{bmatrix} \tilde{A}^b_{yn} \\ \tilde{A}^c_{yn} \end{bmatrix} + \begin{bmatrix} \frac{\cosh k_n\Delta - 1}{\sinh k_n\Delta} \\ -\frac{\cosh k_n\Delta - 1}{\sinh k_n\Delta} \end{bmatrix} j\mu_0 \tilde{M}_{xn} \tag{10}$$

$$\begin{bmatrix} \tilde{B}^d_{zn} \\ \tilde{B}^e_{zn} \end{bmatrix} = k_n \begin{bmatrix} \coth k_n x_0 & \frac{-1}{\sinh k_n x_0} \\ \frac{1}{\sinh k_n x_0} & -\coth k_n x_0 \end{bmatrix} \begin{bmatrix} \tilde{A}^d_{yn} \\ \tilde{A}^e_{yn} \end{bmatrix} \tag{11}$$

$$\begin{bmatrix} \tilde{B}^f_{zn} \\ \tilde{B}^g_{zn} \end{bmatrix} = k_n \begin{bmatrix} \coth k_n\Gamma & \frac{-1}{\sinh k_n\Gamma} \\ \frac{1}{\sinh k_n\Gamma} & -\coth k_n\Gamma \end{bmatrix} \begin{bmatrix} \tilde{A}^f_{yn} \\ \tilde{A}^g_{yn} \end{bmatrix} - \begin{bmatrix} \frac{\cosh k_n\Gamma - 1}{\sinh k_n\Gamma} \\ -\frac{\cosh k_n\Gamma - 1}{\sinh k_n\Gamma} \end{bmatrix} \frac{\mu_0}{k_n} \tilde{J}_{yn} \tag{12}$$

$$\tilde{B}^h_{zn} = \gamma_n \tilde{A}^h_{yn}. \tag{13}$$

The terms containing $\tilde{M}_{xn}$ and $\tilde{J}_{yn}$ represent sources in the magnet and current regions, respectively. The other source term $\tilde{M}_{zn}$ enters through boundary conditions and does not appear in the transfer relations. Since (11) describes the transfer relations in free space, it has no source term. Equations (9) and (13) account for the half-infinite regions above and below the boundaries (a) and (h), respectively.

These transfer relations express the constraints on field and potential quantities imposed by the MQS form of Maxwell's equations. In our case, the transfer relations give eight equations in sixteen unknowns. In order to solve for the field quantities, eight more independent equations are required. These come from the boundary conditions on field and potential at each of the four boundaries; these conditions are given in Appendix A. Using these conditions, the fields at the boundary (d) can be obtained as follows

$$\tilde{H}^d_{xn} = \frac{j}{2k_n} \tilde{J}_{yn} e^{-\gamma_n x_0} \left(1 - e^{-\gamma_n \Gamma}\right) e^{-jk_n z_0} + \left(-\frac{jk_n}{2\gamma_n} \tilde{M}_{zn} + \frac{1}{2} \tilde{M}_{xn}\right) \left(1 - e^{-\gamma_n \Delta}\right) \tag{14}$$

$$\tilde{H}^d_{zn} = -\frac{1}{2\gamma_n} \tilde{J}_{yn} e^{-\gamma_n x_0} \left(1 - e^{-\gamma_n \Gamma}\right) e^{-jk_n z_0} + \left(-\frac{1}{2} \tilde{M}_{zn} - \frac{j\gamma_n}{2k_n} \tilde{M}_{xn}\right) \left(1 - e^{-\gamma_n \Delta}\right). \tag{15}$$

B. Forces

In this section we describe the force acting on the magnet array due to the stator excitation currents. This force is derived via Maxwell stress tensor [15]. As presented in [12], the stress tensor T_{ij} for magnetically linear materials associated with the Korteweg-Helmholtz force density is

$$T_{ij} = \mu H_i H_j - \delta_{ij} \frac{\mu}{2} H_k H_k \tag{16}$$

using the Einstein summation convention where since the k's appear twice in the same term they are to be summed from one to three. The Kronecker delta δ_{ij} is 0 when $i \neq j$, and is 1 when $i = j$. The force acting on a volume of the magnet array is given by the integral of the stress tensor over the surface of the volume. For a spatially-periodic structure, the integration is simplified if the volume encloses an integer number of periods. In this case the components on the z-faces of the volume cancel due to symmetry. We can consider the upper surface of the volume to extend to infinity, where the fields are zero and thus the only contribution is along the bottom surface which we take to lie on boundary (d).

If the lower surface encloses an integer number of periods and is of area S, then the x-directed force acting on the enclosed section of magnet array is given by

$$F_x = -S\left\langle T^d_{xx} \right\rangle_z = -\frac{S\mu_0}{2} \left\langle H^d_x H^d_x - H^d_z H^d_z \right\rangle_z, \tag{17}$$

and the z-directed force acting on the enclosed section of magnet array is given by

$$F_z = -S\left\langle T^d_{xz} \right\rangle_z = -S\mu_0 \left\langle H^d_x H^d_z \right\rangle_z, \tag{18}$$

where the angle bracket expression $\langle \cdot \rangle_z$ indicates the spatial average on z of the quantity enclosed by the brackets. The minus sign appears because the bottom surface has an outwardly-directed normal in the $-x$-direction. A useful identity is the spatial averaging theorem (Section 2.15 of [12])

$$\left\langle \sum_{n=-\infty}^{\infty} \tilde{A}_n e^{-jk_n z} \sum_{m=-\infty}^{\infty} \tilde{B}_m e^{-jk_m z} \right\rangle_z = \sum_{n=-\infty}^{\infty} \tilde{A}_n \tilde{B}_{-n} = \sum_{n=-\infty}^{\infty} \tilde{A}_n \tilde{B}^*_n \tag{19}$$

where the last step holds if the Fourier series represents a real function since the components must then possess conjugate symmetry.

Although the analysis can be carried out more generally, in the following we assume that the stator currents are sinusoidally distributed with a fundamental period of l and thus that $\tilde{J}_n$ is equal to zero for $n \neq \pm 1$. Specifically, we let $\tilde{J}_1 = J_a + jJ_b$, and $\tilde{J}_{-1} = J_a - jJ_b$. That is, $2J_a$ is the peak phase A current density and $2J_b$ is the peak phase B current density. The above assumption is reasonable since it is primarily the fundamental field components which are responsible for force production. Further, in application, the spatial currents are driven to resemble a sinusoid and thus the assumption is accurate for our purposes. Under this assumption, applying (19) to (17) and (18), and using (14) and (15) yield, after some algebra, the forces acting on one pitch of the magnet array as

$$\begin{bmatrix} F_{x\lambda} \\ F_{z\lambda} \end{bmatrix} = \mu_0 M_0 G e^{-\gamma_1 x_0} \begin{bmatrix} -\sin\gamma_1 z_0 & \cos\gamma_1 z_0 \\ \cos\gamma_1 z_0 & \sin\gamma_1 z_0 \end{bmatrix} \begin{bmatrix} J_a \\ J_b \end{bmatrix} \tag{20}$$

where $F_{x\lambda}$ and $F_{z\lambda}$ are the x-directed and z-directed forces per spatial wavelength, respectively. Here $\mu_0 M_0$ is the remanence of the permanent magnets. The constant

$$G = \frac{\sqrt{2}wl^2}{\pi^2} \left(1 - e^{-\gamma_1 \Gamma}\right) \left(1 - e^{-\gamma_1 \Delta}\right) \tag{21}$$

contains the effects of the motor geometry. The x_0 and z_0 dependencies have been explicitly retained since these variables represent motion of the magnet array relative to the stator.

C. Electrical Terminal Relation

In order to derive the electrical terminal relation, we use the Faraday induction law

$$\oint_C \mathbf{E}\cdot d\mathbf{l} = -\frac{d}{dt}\int_S \mathbf{B}\cdot d\mathbf{a}. \tag{22}$$

Here the integration is taken along a contour fixed in the nonmoving frame (or the nonprimed frame in Fig. 1). The magnetic flux density $\mathbf{B}$ inside the integral on the right hand side in (22) consists of the flux densities due to the magnet ${}^{M}\mathbf{B}$ and due to the stator ${}^{S}\mathbf{B}$. It can be shown that this integral can be expanded for two-dimensional geometries as

$$\begin{aligned} -V_s + \oint_C \frac{\mathbf{J}_f}{\sigma}\cdot d\mathbf{l} + \oint_C \left(-v_x {}^{M}B_z + v_z {}^{M}B_x\right)\mathbf{i}_y \cdot d\mathbf{l} \\ = -\frac{d}{dt}\int_S {}^{S}\mathbf{B}\cdot d\mathbf{a}. \end{aligned} \tag{23}$$

The first term is the driving voltage. The second term is Ohmic drop denoted as $R_S I_S$. The third term is the back electromotive force (emf), or speed voltage. Here, $v_x \equiv \frac{dx_0}{dt}$ and $v_x \equiv \frac{dz_0}{dt}$ are the velocities of the magnet array in the x- and z-directions, respectively. The right-hand-side term is the induced voltage due to self- and mutual-inductance of the stator coil. This terminal relation gives a complete electrical model for the linear motor. The rest of this section gives detailed derivations of the last two terms of (23).

1) Stator Flux Linkage: The vector potential simplifies the evaluation of the flux passing through a surface. The magnetic flux Φ linked by a closed surface S is given by the integration of the magnetic flux density over S. By the Stokes' theorem, this can be represented as the line integral of vector potential $\mathbf{A}$ around the contour C enclosing the surface, i.e.,

$$\Phi = \int_S \mathbf{B}\cdot d\mathbf{a} = \int_S (\nabla\times\mathbf{A})\cdot d\mathbf{a} = \oint_C \mathbf{A}\cdot d\mathbf{l}. \tag{24}$$

In the two-dimensional geometry of our model, the path of the line integral of interest is confined to a plane and is a rectangle. This situation is depicted in Fig. 2. As seen in the figure, we have constructed a six-phase machine where in the windings occupy rectangular windings of thickness Γ and width $l/2\phi$, where l is the pitch and ϕ is the number of phases of the machine. In our model, the vector potential $\mathbf{A}$ has only a y-component which is constant in y. This enables us to readily evaluate Φ for every surface closed by the path C inside the stator current distribution. Since the winding and its return path are separated by half the pitch, the flux linked by a winding lying at x, z and $x, z + l/2$ is

$$\Phi = \sum_{n=-\infty}^{\infty}\left[\tilde{A}_{yn}(x)e^{-jk_n z} - \tilde{A}_{yn}(x)e^{-jk_n(z+l/2)}\right]w \tag{25}$$

where w is the depth of the stator winding.

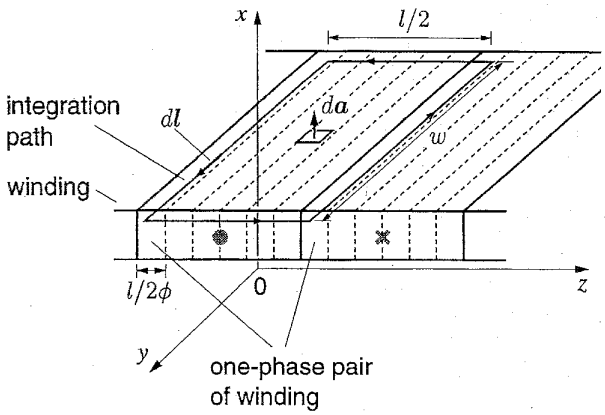

Fig. 2. Closed contour for magnetic flux.

If the turn distribution is uniform with η_0 turns per unit cross-sectional area, then there are $\eta_0 dxdz$ turns in an infinitesimal area. The total flux linked by the one phase winding for one pitch l is given by the integration of the linked infinitesimal flux over one pitch of the winding (Fig. 2)

$$\lambda = w\eta_0 \sum_{n=-\infty,\text{odd}}^{\infty}\int_0^{l/2\phi} 2e^{-jk_n z}dz \int_0^{\Gamma}\tilde{A}_{yn}(x)dx. \tag{26}$$

2) Self-Inductance: Let us derive a formula for a six-phase winding ($\phi = 6$) as in Fig. 2. From (26), following some algebra, the total flux linkage in terms of the current density may be expressed as

$$\begin{aligned} \lambda_S = {} & \frac{j\mu_0 w\eta_0 l}{\pi} \\ & \cdot \sum_{n=-\infty,\text{odd}}^{\infty}\frac{\tilde{J}_{yn}}{nk_n^2}\left(e^{-j\pi n/6}-1\right)\left(\Gamma + \frac{e^{-\gamma_n\Gamma}-1}{\gamma_n}\right). \end{aligned} \tag{27}$$

The Fourier coefficients of the current density with the amplitude J_0 for the first phase out of six can be shown as

$$\tilde{J}_{yn} = \begin{cases} \frac{J_0}{j\pi n}\left(e^{j\pi n/6}-1\right), & n\text{: odd} \\ 0, & n\text{: even} \end{cases}. \tag{28}$$

Substituting this into (27) yields

$$\begin{aligned} \lambda_S = {} & \frac{\mu_0 w\eta_0 l^3 J_0}{2\pi^4} \\ & \cdot \sum_{n=-\infty,\text{odd}}^{\infty}\frac{1}{n^4}\left(1-\cos\frac{\pi}{6}n\right)\left(\Gamma + \frac{e^{-\gamma_n\Gamma}-1}{\gamma_n}\right). \end{aligned} \tag{29}$$

Let $J_0 = \eta_0 I_S$, where I_S is the stator winding current. Then the self-inductance of one phase winding per pitch is, via $\lambda_S = L_S I_S$, given by

$$\begin{aligned} L_S = {} & \frac{\mu_0 w\eta_0^2 l^3}{2\pi^4} \\ & \cdot \sum_{n=-\infty,\text{odd}}^{\infty}\frac{1}{n^4}\left(1-\cos\frac{\pi}{6}n\right)\left(\Gamma + \frac{e^{-\gamma_n\Gamma}-1}{\gamma_n}\right). \end{aligned} \tag{30}$$

We use this formula to estimate self-inductance of an example motor winding later in this section.

3) Back Electromotive Force: Following an analysis similar to the previous section the back emf of one pitch is given by

$$V_{\text{bemf}} = 2w\eta_0 \sum_{n=-\infty}^{\infty} \left\{ -v_x \left(-\frac{\mu_0}{2}\tilde{M}_{zn} - \frac{j\gamma_n\mu_0}{2k_n}\tilde{M}_{xn} \right) + v_z \left(-\frac{jk_n\mu_0}{2\gamma_n}\tilde{M}_{zn} + \frac{\mu_0}{2}\tilde{M}_{xn} \right) \right\} \cdot \left(1 - e^{-\gamma_n\Delta}\right) e^{-\gamma_n(x_0+\Gamma)} e^{jk_n z_0} \cdot \int_0^{l/2\phi} e^{-jk_n z} dz \int_0^{\Gamma} e^{\gamma_n x} dx. \quad (31)$$

We can specifically derive the back emf for a six-phase motor ($\phi = 6$) with evaluations of the integrals. The back emf per pitch at the stator terminals of a one-phase winding denoted in Fig. 2 then reduces to

$$V_{\text{bemf}} = w\eta_0 \sum_{n=-\infty,\text{odd}}^{\infty} \left(\frac{\mu_0}{\gamma_n}\tilde{M}_{zn} + \frac{j\mu_0}{k_n}\tilde{M}_{xn} \right) \cdot \left(j\frac{v_x}{k_n} + \frac{v_z}{\gamma_n} \right) \left(1 - e^{-\gamma_n\Delta}\right)\left(1 - e^{-\gamma_n\Gamma}\right) \cdot \left(e^{-j\pi n/6} - 1\right) e^{-\gamma_n x_0} e^{jk_n z_0}. \quad (32)$$

This completes the exposition of the electrical terminal relation given in (23). In the following we give experimental verifications to the above analytical results.

D. Prototype Levitator and Experimental Verifications

A six-degree-of-freedom magnetically levitated x-y stage has been constructed which uses electromagnets to control the motion of a 13.5-kg platen in five (three rotational and two translational) degrees of freedom and a permanent-magnet linear motor to control motion in the sixth degree of freedom (Fig. 3). For fine focusing the stage can provide 400 μm of travel normal to the wafer surface and milliradian rotations around three axes. The linear motor consists of a permanent-magnet Halbach array attached to the underside of the platen and a linear ironless six-phase stator fixed in the machine frame. A conventional mechanical linear slide will be used to provide 200 mm of travel in the y-direction. A preliminary 500-nm step response in the z-axis is shown in Fig. 4. The position of the stage in the z-direction is read with a laser interferometer with 0.6 nm of position resolution.

The parameters of the motor are the following: number of phases, $\phi = 6$; number of turns per phase: 80 (#22 copper wire); turn density, $\eta_0 = 1.86 \times 10^6$ turns/m^2; pitch, $l = 5.08$ cm (2 in); depth, $w = 15$ cm; winding thickness, $\Gamma = l/5$; magnet-array thickness, $\Delta = l/4$. A winding has 44-cm average turn length; its average end-turn length is 14 cm. The total winding resistance and self-inductance for one phase are 19.8 Ω and 9.48 mH, respectively. The stator has 10 pitches of winding (total length of 50.8 cm). The magnet array consists of $5\frac{1}{4}$ pitches (21 rows of 0.5 × 0.5-in magnets) of NdFeB material with remanence $\mu_0 M_0 = 1.1$ T.

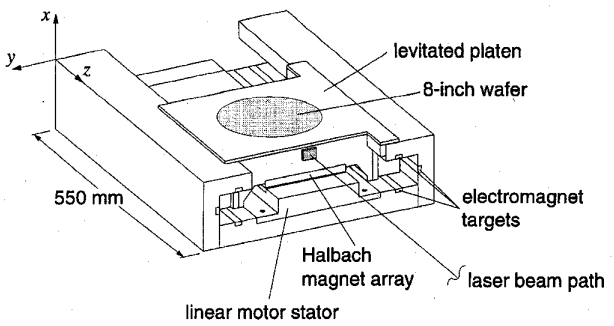

Fig. 3. Six degree-of-freedom magnetically levitated stage.

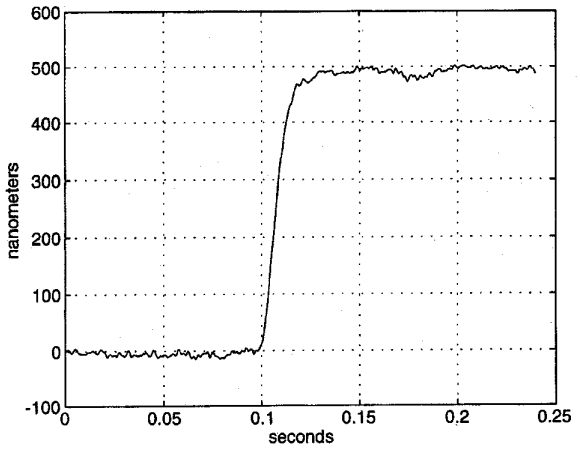

Fig. 4. 500-nm step response.

With the motor geometry given above we can estimate the self-inductance of a stator winding directly with (30). Since (30) gives self-inductance per pitch, we need to multiply it by the number of pitches of winding which is 10 in this case. Our analysis predicts a total self-inductance of 6.27 mH for a phase. The actual inductance measured by a dynamic signal analyzer is 9.48 mH. In spite of this 34% error, they are in good agreement considering that the analysis ignores the winding end turns (32% of the total length) which connect the successive phase sections. These end turns likely account for the larger measured inductance.

An experimental wave form for the back emf of one phase is shown in Fig. 5. These data were acquired as follows. During the experiment the platen is suspended in five degrees of freedom. The driving circuits for the linear motor are disconnected. The platen is then pushed by hand while the voltage on one phase is recorded. The air gap between the magnet array and the stator winding is maintained at 400 μm. The velocity along the z-axis is estimated graphically as $v_z = 160$ mm/s. On the basis of the fundamental terms ($n = \pm 1$) of the square Halbach array's Fourier coefficients, $\tilde{M}_{x,\pm 1} = \frac{\sqrt{2}M_0}{\pi}$ and $\tilde{M}_{z,\pm 1} = \pm j\frac{\sqrt{2}M_0}{\pi}$, we predict the peak magnitude of the back emf should be 1.6 V per phase via (32). Since the magnet array consists of $5\frac{1}{4}$ pitches, the total effective back emf is estimated as 8.4 V. The actual data yield about 8 V. The end and edge effects in the magnet and winding

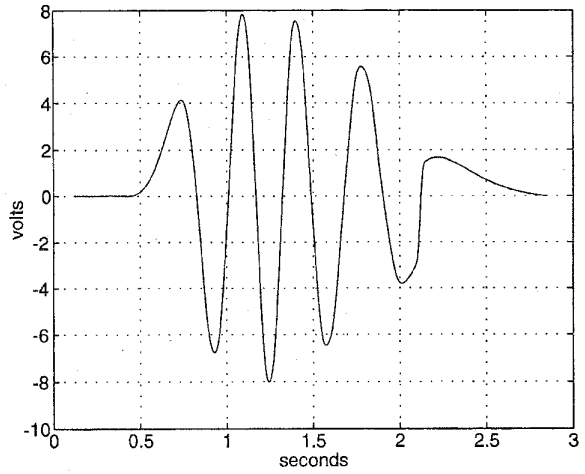

Fig. 5. Back emf wave form.

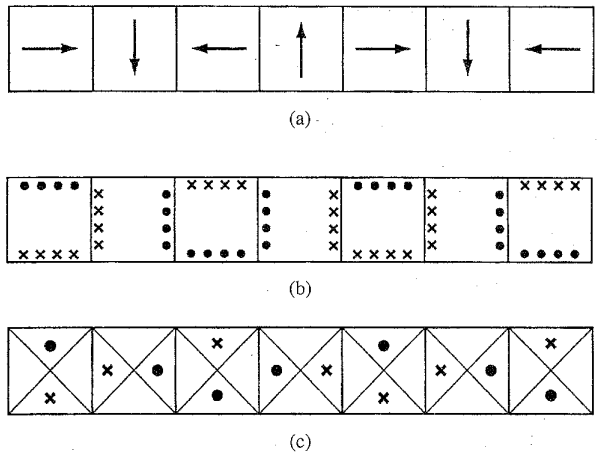

Fig. 6. Electromagnetic dual of Halbach array. (a) Halbach magnet array. (b) Equivalent current model. (c) Triangular winding pattern.

may be primarily responsible for the decrease of the magnitude in the real experiment. That is, the effective flux density linked by the winding is less for the real motor than that predicted by the idealized theory.

IV. Single-Sided Field Design

Halbach developed a single-sided rare-earth cobalt magnet array for use in undulators and particle accelerators [16]. The use of Halbach magnet arrays for motor design is presented in [14]. It is shown there that the square Halbach array has $\sqrt{2}$ times stronger field than that of more conventional ironless magnet arrays with the same volume. The earlier work [14] alluded to, but did not develop analytical results for single-sided electromagnets which are the analog of the Halbach magnet array [9]. This kind of winding pattern may have applications where it is desirable to build a single-sided electromagnet such as in maglev trains. A possible winding pattern for such an electromagnet is illustrated in Fig. 6(c). The figure shows the winding's analogy with the Halbach magnet array through the relationship $\mathbf{K}_e = \mathbf{n} \times [\mathbf{M}^a - \mathbf{M}^b]$. Since it is not possible to implement true surface currents, the winding pattern occupies the volume of the triangular regions shown.

This single-sided winding pattern can be readily analyzed using the approach presented above. Summarizing this result, the fundamental Fourier component of the normal magnetic flux density due to such a triangular stator current distribution is

$$\tilde{B}^e_{x1} = -\frac{\mu_0 J_0}{\sqrt{2}\pi}\left[\frac{1-e^{-\gamma_1\Gamma}}{\gamma_1} - \frac{1}{\left(\frac{\pi}{2\Gamma}\right)^2+\gamma_1^2}\left(2\gamma_1 + \frac{\pi}{\Gamma}e^{-\gamma_1\Gamma}\right)\right] \tag{33}$$

and

$$\tilde{B}^h_{x1} = -\frac{\mu_0 J_0}{\sqrt{2}\pi}\left[\frac{1-e^{-\gamma_1\Gamma}}{\gamma_1} + \frac{1}{\left(\frac{\pi}{2\Gamma}\right)^2+\gamma_1^2}\left(2\gamma_1 e^{-\gamma_1\Gamma} - \frac{\pi}{\Gamma}\right)\right] \tag{34}$$

at the boundaries (e) and (h), respectively. Here, J_0 is magnitude of the current density within the triangular regions shown.

The weak side (h) of the winding has no fundamental field under the condition that the pitch l is four times as long as the thickness Γ. This is so, since if we use $\gamma_1 = 2\pi/l$ and substitute $l = 4\Gamma$ into (34) we get $\tilde{B}^h_{x1} = 0$. Similarly, in this case the fundamental of the tangential field $\tilde{B}^h_{z1}$ is also zero on the weak side of the electromagnet. We can further show that the third harmonic for the strong side vanishes under the same condition, and thus the next harmonic on the strong side is the fifth. Thus the strong-side field is highly sinusoidal. This would yield smoother operation if the motor were used in a linear motor, e.g., for a maglev train.

The configuration of the winding for two-phase operation is shown in Fig. 7. Here, phase 2 is spatially displaced by 90° from phase 1. Fig. 8 shows the stator magnetic flux lines for this configuration as solved for via finite-element analysis software. Although the electromagnet shown here is of finite extent, we can see the resulting effectively single-sided flux line pattern. We find, however, that the major disadvantage is that the winding is less power efficient than those reported earlier [14]. Thus this single-sided winding is not likely to be used in power-sensitive applications in conventional machines. However, in superconducting machines this winding pattern, or others like it, may prove to be of interest.

V. Conclusion

The main purpose of this paper is to provide a general design and analysis framework for linear permanent-magnet machines. The models resulting from this analysis serve as design tools for the development of high-resolution, power-efficient positioning stages. To show the application of these design tools we have presented the electromechanical characteristics of an example magnetic levitator. The motor fields, forces, and electrical terminal relation are given. We provide experimental measurements of self-inductance and back emf. In good agreement with the estimated values from the analyses,

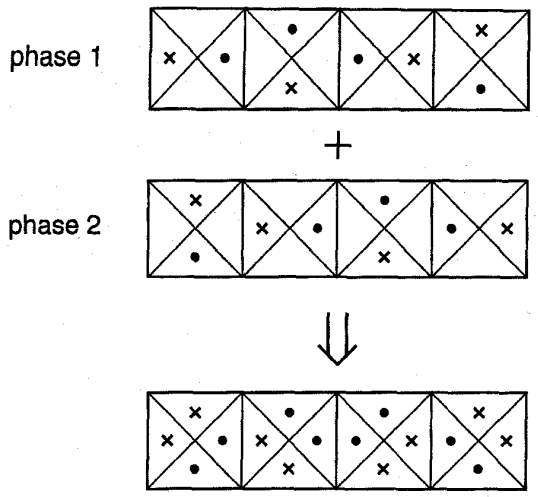

Fig. 7. Two-phase operation.

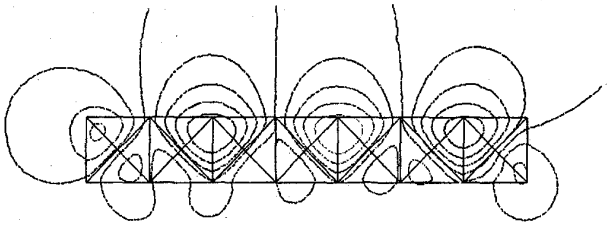

Fig. 8. Flux lines.

the experimental results confirm the validity of the design and analysis framework.

Our framework is general in the sense that it can address complex magnet arrays and winding patterns. For example, a triangular winding pattern which has a primarily single-sided magnetic field is developed and analyzed.

APPENDIX A
FIELD CALCULATIONS

1) Field Due to Magnet: There is no free current in the magnet region in Fig. 1. So, $\nabla \times \mathbf{H} = \mathbf{J}_f = 0$, and $\nabla \times \mathbf{B} = \mu_0 \nabla \times \mathbf{M}$. The vector potential satisfies the scalar Poisson equation for y-component in the Cartesian coordinate

$$\frac{\partial^2}{\partial z^2} A_{yn} = -\mu_0 [\nabla \times \mathbf{M}_n]_y \tag{35}$$

where $\mathbf{M}_n$ is the nth order Fourier component of $\mathbf{M}$. Taking the curl of the nth magnetization term,

$$\nabla \times \mathbf{M}_n = -jk_n \tilde{M}_{xn} e^{-jk_n z'} \mathbf{i}_y. \tag{36}$$

Let $A_{yn} = A_{ynp} + A_{ynh}$, where A_{ynp} is the particular part of the solution and A_{ynh} is the homogeneous part. Solving the Poisson equation for A_{yn},

$$\tilde{A}_{ynp} = -\frac{j\mu_0}{k_n} \tilde{M}_{xn}. \tag{37}$$

Since the potential must depend on hyperbolic trigonometric function, the homogeneous solution inside the magnet region takes the following form by the general Laplace equation's solution

$$\tilde{A}_{ynh} = \left(\tilde{A}^b_{yn} + \frac{j\mu_0}{k_n} \tilde{M}_{xn} \right) \frac{\sinh k_n x'}{\sinh k_n \Delta} - \left(\tilde{A}^c_{yn} + \frac{j\mu_0}{k_n} \tilde{M}_{xn} \right) \frac{\sinh k_n (x' - \Delta)}{\sinh k_n \Delta}. \tag{38}$$

From the definition of the vector potential $\mathbf{B} \equiv \nabla \times \mathbf{A}$

$$\tilde{B}_{xn} = -\frac{\partial}{\partial z} \tilde{A}_{yn} = jk_n \tilde{A}_{yn} \tag{39}$$

$$\tilde{B}_{zn} = \frac{\partial}{\partial x} \tilde{A}_{yn}. \tag{40}$$

Now from (40)

$$\tilde{B}_{zn} = k_n \left(\tilde{A}^b_{yn} + \frac{j\mu_0}{k_n} \tilde{M}_{xn} \right) \frac{\cosh k_n x'}{\sinh k_n \Delta} - k_n \left(\tilde{A}^c_{yn} + \frac{j\mu_0}{k_n} \tilde{M}_{xn} \right) \frac{\cosh k_n (x' - \Delta)}{\sinh k_n \Delta}. \tag{41}$$

Evaluated at the boundaries (b) $(x' = \Delta)$ and (c) $(x' = 0)$, the transfer relations are

$$\begin{bmatrix} \tilde{B}^b_{zn} \\ \tilde{B}^c_{zn} \end{bmatrix} = k_n \begin{bmatrix} \coth k_n \Delta & \frac{-1}{\sinh k_n \Delta} \\ \frac{1}{\sinh k_n \Delta} & -\coth k_n \Delta \end{bmatrix} \begin{bmatrix} \tilde{A}^b_{yn} \\ \tilde{A}^c_{yn} \end{bmatrix} + \begin{bmatrix} \frac{\cosh k_n \Delta - 1}{\sinh k_n \Delta} \\ -\frac{\cosh k_n \Delta - 1}{\sinh k_n \Delta} \end{bmatrix} j\mu_0 \tilde{M}_{xn}. \tag{42}$$

Using the limits $\lim_{x \to \pm\infty} \coth x = \pm 1$ and $\lim_{x \to \pm\infty} \sinh x = \pm\infty$ (The order of the signs is significant.), the transfer relations for the half-infinite regions above the surface (a) and below the surface (d) can be derived from (42)

$$\tilde{B}^a_{zn} = -\gamma_n \tilde{A}^a_{yn} \tag{43}$$

$$\tilde{B}^d_{zn} = \gamma_n \tilde{A}^d_{yn}. \tag{44}$$

Since there is no impulse of field (i.e., no current doublet) everywhere, the vector potential is continuous at the boundaries

$$\tilde{A}^a_{yn} = \tilde{A}^b_{yn} \tag{45}$$

$$\tilde{A}^c_{yn} = \tilde{A}^d_{yn}. \tag{46}$$

The equivalent surface current densities at the boundary (b) and (c) are

$$\mathbf{K}^b_{yn} = \mathbf{M}_n \times \mathbf{i}_x = \tilde{M}_{zn} e^{-jk_n z'} \mathbf{i}_y \tag{47}$$

$$\mathbf{K}^c_{yn} = \mathbf{M}_n \times (-\mathbf{i}_x) = -\tilde{M}_{zn} e^{-jk_n z'} \mathbf{i}_y. \tag{48}$$

So, the boundary conditions for magnetic flux density are

$$-\tilde{B}^a_{zn} + \tilde{B}^b_{zn} = \mu_0 \tilde{M}_{zn} \tag{49}$$

$$-\tilde{B}^c_{zn} + \tilde{B}^d_{zn} = -\mu_0 \tilde{M}_{zn}. \tag{50}$$

Solving the system of algebraic equations (42)–(46) and (49) and (50) yields

$$\tilde{A}^a_{yn} = \left(\frac{\mu_0}{2\gamma_n} \tilde{M}_{zn} - \frac{j\mu_0}{2k_n} \tilde{M}_{xn} \right) \left(1 - e^{-\gamma_n \Delta} \right) \tag{51}$$

$$\tilde{A}^d_{yn} = \left(-\frac{\mu_0}{2\gamma_n} \tilde{M}_{zn} - \frac{j\mu_0}{2k_n} \tilde{M}_{xn} \right) \left(1 - e^{-\gamma_n \Delta} \right). \tag{52}$$

From (39) and (44), and using (52), we find

$$\tilde{B}^d_{xn} = \left(-\frac{jk_n\mu_0}{2\gamma_n}\tilde{M}_{zn} + \frac{\mu_0}{2}\tilde{M}_{xn}\right)\left(1 - e^{-\gamma_n\Delta}\right) \quad (53)$$

$$\tilde{B}^d_{zn} = \left(-\frac{\mu_0}{2}\tilde{M}_{zn} - \frac{j\gamma_n\mu_0}{2k_n}\tilde{M}_{xn}\right)\left(1 - e^{-\gamma_n\Delta}\right). \quad (54)$$

Equations (52)–(54) are the field and potential solution for the magnet at the boundary (d) as given in the body of the paper.

2) Field Due to Stator Current: In the stator current region, the governing equation is

$$\frac{\partial^2}{\partial z^2}A_{ynp} = -\mu_0[\mathbf{J}_f]_y = -\mu_0\tilde{J}_{yn}e^{-jk_nz}. \quad (55)$$

A particular solution of the above Poisson equation is

$$\tilde{A}_{ynp} = \frac{\mu_0}{k_n^2}\tilde{J}_{yn}. \quad (56)$$

Through similar steps as in the magnet case, we obtain the transfer relations for the stator current

$$\begin{bmatrix}\tilde{B}^f_{zn}\\ \tilde{B}^g_{zn}\end{bmatrix} = k_n\begin{bmatrix}\coth k_n\Gamma & \frac{-1}{\sinh k_n\Gamma}\\ \frac{1}{\sinh k_n\Gamma} & -\coth k_n\Gamma\end{bmatrix}\begin{bmatrix}\tilde{A}^f_{yn}\\ \tilde{A}^g_{yn}\end{bmatrix} - \begin{bmatrix}\frac{\cosh k_n\Gamma - 1}{\sinh k_n\Gamma}\\ -\frac{\cosh k_n\Gamma - 1}{\sinh k_n\Gamma}\end{bmatrix}\frac{\mu_0}{k_n}\tilde{J}_{yn}. \quad (57)$$

Transfer relations for the half-infinite region are as in the magnet case

$$\tilde{B}^e_{zn} = -\gamma_n\tilde{A}^e_{yn} \quad (58)$$

$$\tilde{B}^h_{zn} = \gamma_n\tilde{A}^h_{yn}. \quad (59)$$

Vector potential is continuous at the boundaries,

$$\tilde{A}^e_{yn} = \tilde{A}^f_{yn} \quad (60)$$

$$\tilde{A}^g_{yn} = \tilde{A}^h_{yn}. \quad (61)$$

Since there is no surface current on surfaces of the stator, the horizontal component of magnetic flux density is continuous

$$-\tilde{B}^e_{zn} + \tilde{B}^f_{zn} = 0 \quad (62)$$

$$-\tilde{B}^g_{zn} + \tilde{B}^h_{zn} = 0. \quad (63)$$

Solving the system of algebraic equations (57)–(63) yields

$$\tilde{A}^e_{yn} = \frac{\mu_0}{2k_n^2}\tilde{J}_{yn}\left(1 - e^{-\gamma_n\Gamma}\right) \quad (64)$$

$$\tilde{A}^h_{yn} = \frac{\mu_0}{2k_n^2}\tilde{J}_{yn}\left(1 - e^{-\gamma_n\Gamma}\right). \quad (65)$$

From (58) and with $k_n^2 = \gamma_n^2$

$$\tilde{B}^e_{xn} = jk_n\tilde{A}^e_{yn} = \frac{j\mu_0}{2k_n}\tilde{J}_{yn}\left(1 - e^{-\gamma_n\Gamma}\right) \quad (66)$$

$$\tilde{B}^e_{zn} = -\frac{\mu_0}{2\gamma_n}\tilde{J}_{yn}\left(1 - e^{-\gamma_n\Gamma}\right). \quad (67)$$

Using the transfer relations for the air gap (11), we can show the total fields due to the magnet and the stator current are as given in (14) and (15).

3) Vector Potential Inside Stator: First, let us calculate the vector potential at the stator boundary (e), ${}^M\tilde{A}^e_{yn}(= {}^M\tilde{A}^f_{yn})$ due to the magnet. From (11), $\tilde{B}^d_{zn} = k_n\coth k_nx_0\ \tilde{A}^d_{yn} - \frac{k_n}{\sinh k_nx_0}\tilde{A}^e_{yn}$, and then,

$$\tilde{A}^e_{yn} = \cosh k_nx_0\tilde{A}^d_{yn} - \frac{\sinh k_nx_0}{k_n}\tilde{B}^d_{zn}. \quad (68)$$

Using (52) and (54) and with some intermediate steps, vector potential represented in the origin of nonprimed xyz-frame is given by

$${}^M\tilde{A}^e_{yn} = \left(-\frac{\mu_0}{2\gamma_n}\tilde{M}_{zn} - \frac{j\mu_0}{2k_n}\tilde{M}_{xn}\right)e^{-\gamma_nx_0}\cdot e^{jk_nz_0}\left(1 - e^{-\gamma_n\Delta}\right). \quad (69)$$

The vector potential at the stator boundaries due to stator current are from (64) and (65)

$${}^S\tilde{A}^e_{yn} = {}^S\tilde{A}^h_{yn} = \frac{\mu_0}{2k_n^2}\tilde{J}_{yn}\left(1 - e^{-\gamma_n\Gamma}\right). \quad (70)$$

Now we think of an imaginary boundary at $x = X$ and calculate the vector potential there. Let the boundary upper and lower surfaces be (p) and (q), respectively. Vector potentials due to the current in the upper section $(X \le x \le \Gamma)$ and the lower section $(0 \le x \le X)$ come directly from (64) and (65) as

$${}^S_U\tilde{A}^p_{yn}\left(= {}^S_U\tilde{A}^q_{yn}\right) = \frac{\mu_0}{2k_n^2}\tilde{J}_{yn}\left(1 - e^{-\gamma_n(\Gamma - X)}\right) \quad (71)$$

$${}^S_L\tilde{A}^p_{yn}\left(= {}^S_L\tilde{A}^q_{yn}\right) = \frac{\mu_0}{2k_n^2}\tilde{J}_{yn}\left(1 - e^{-\gamma_nX}\right). \quad (72)$$

By superposition, the vector potential inside the stator at $x = X$ is the sum of ${}^S_U\tilde{A}^p_{yn}$ and ${}^S_L\tilde{A}^p_{yn}$

$${}^S\tilde{A}^p_{yn} = \frac{\mu_0}{2k_n^2}\tilde{J}_{yn}\left(2 - e^{-\gamma_nX} - e^{-\gamma_n(\Gamma - X)}\right). \quad (73)$$

Thus, the total vector potential at (p) due to the magnet and the current is from (69) and (73)

$$\tilde{A}^p_{yn} = \left(-\frac{\mu_0}{2\gamma_n}\tilde{M}_{zn} - \frac{j\mu_0}{2k_n}\tilde{M}_{xn}\right)\cdot e^{-\gamma_n(x_0 + \Gamma - X)}e^{jk_nz_0}\left(1 - e^{-\gamma_n\Delta}\right) + \frac{\mu_0}{2k_n^2}\tilde{J}_{yn}\left(2 - e^{-\gamma_nX} - e^{-\gamma_n(\Gamma - X)}\right). \quad (74)$$

This result is used to calculate flux linkage and self-inductance of the winding.

ACKNOWLEDGMENT

The authors wish to acknowledge Jeffrey H. Lang and John Ofori-Tenkorang of the MIT Laboratory for Electromagnetic and Electronic Systems for their helpful discussions especially with regard to the single-sided field design material.

REFERENCES

[1] B. A. Sawyer, "Magnetic positioning device," U.S. Patent 3 376 578, Apr. 1968.

[2] W. E. Hinds and B. Nocito, "The Sawyer linear motor," in *Proc. 2nd Symp. Incremental Motion Contr. Syst., Devices*, 1973, pp. W-1–W-10.

[3] E. R. Pelta, "Two axis Sawyer motor," in *Proc. 12th Annu. IEEE Ind. Electron. Soc. Conf.*, 1986, pp. 3–8.

[4] T. Asakawa, "Two dimensional precise positioning devices for use in a semiconductor apparatus," U.S. Patent 4 535 278, Aug. 1985.

[5] W. E. Hinds, "Single plane orthogonally movable drive system," U.S. Patent 4 654 571, Mar. 1987.

[6] D. Ebihara and M. Watada, "Study of a basic structure of surface actuator," *IEEE Tran Magn.*, vol. 25, no. 5, pp. 3916–3918, 1989.

[7] J. D. Buckley, D. N. Galburt, and C. Karatzas, "Step-and-scan lithography using reduction optics," *J. Vacuum Sci., Technol. B*, vol. 7, no. 6, pp. 1607–1612, 1989.

[8] T. Higuchi and H. Kawakatsu, "Development of a magnetically suspended stepping motor for clean-room transportation and sample handling," in *Proc. 11th Int. Conf. Magnetically Levitated Syst., Linear Drives, Maglev '89*, 1989, pp. 363–368.

[9] K. Halbach, "Design of permanent multipole magnets with oriented rare earth cobalt material," *Nuclear Instruments and Methods*, vol. 169, no. 1, pp. 1–10, 1980.

[10] M. Marinescu and N. Marinescu, "New concept of permanent magnet excitation for electrical machines, analytical and numerical computation," *IEEE Trans Magn.*, vol. 28, no. 2, pp. 1390–1393, 1992.

[11] M. G. Abele, H. Rusinek, and F. Bertora, "Field computation in permanent magnets," *IEEE Trans. Magn.*, vol. 28, no. 1, pp. 931–934, 1992.

[12] J. R. Melcher, *Continuum Electromechanics*. Cambridge, MA: MIT Press, 1981.

[13] H. A. Haus and J. R. Melcher, *Electromagnetic Fields and Energy*, Englewood Cliffs, NJ: Prentice-Hall, 1989.

[14] D. L. Trumper, M. E. Williams, and T. H. Nguyen, "Magnet arrays for synchronous machines," in *Proc. IEEE IAS 28th Annu. Meet.*, Oct. 1993, pp. 9–18.

[15] H. H. Woodson and J. R. Melcher, *Electromechanical Dynamics*. New York: Wiley, 1968.

[16] K. Halbach, "Application of permanent magnets in accelerators and electron storage rings," *J. Appl. Phys.*, vol. 57, no. 8, pp. 3605–3608, 1985.

David L. Trumper (S'80–M'90) received the B.S., M.S., and Ph.D. degrees from MIT in Electrical Engineering and Computer Science, in 1980, 1984, and 1990, respectively.

Following the Bachelor's degree, he worked two years for the Hewlett-Packard Co. After finishing the Master's degree, he worked for two years for the Waters Chromatography Division of Millipore. After receiving the Ph.D. degree, he was Assistant Professor in the Electrical Engineering Department at the University of North Carolina at Charlotte for three years, working within the precision engineering group. He joined the MIT Department of Mechanical Engineering in August 1993, and currently is the Rockwell Career Development Assistant Professor. His research interests are in the area of the control of electromechanical systems with a specialization in magnetic suspensions and bearings.

Prof. Trumper is a member of the ASME, ASPE, and JSPE.

Won-jong Kim (S'89) was born in Seoul, Korea, in 1966. He received the B.S. degree (Summa Cum Laude) and M.S. degrees in control and instrumentation engineering from Seoul National University, Seoul, Korea, in 1989 and 1991, respectively. He is a doctoral candidate in electrical engineering and computer science at the Massachusetts Institute of Technology (MIT), Cambridge, MA.

He was awarded a Grand Prix from the Korean Institute of Electrical Engineers' Student Paper Contest in 1988. From 1992 to 1994, he held a Korean Government Overseas Scholarship. His research interests are analysis, design, and real-time control of electromechanical systems. His current concentration is a high-precision magnetic levitator.

Mark E. Williams received the B.S.E.E. and M.S.E.E degrees from the University of North Carolina, Charlotte, NC, in 1990 and 1991, respectively. He is currently working toward the Ph.D. degree in mechanical engineering at the Massachusetts Institute of Technology. Research topics include precision machine design and precision motion control.

Mr. Williams is a member of the American Society of Precision Engineering.